JOURNAL OF MATERIALS SCIENCE **34** (1999) 1611–1618

The formation, structure and properties of nanocrystalline Ni-Mo-B alloys

G. E. ABROSIMOVA, A. S. ARONIN, YU. V. KIR'JANOV, I. I. ZVER'KOVA
Institute of Solid State Physics RAS, Chernogolovka, Russia
E-mail: aronin@issp.ac.ru

V. V. MOLOKANOV
Baikov Institute of Metallurgy RAS, Moscow

H. ALVES, U. KÖSTER
Department of Chemical Engineering, University of Dortmund, Germany

The structure, structure evolution and microhardness of nanocrystalline Ni-Mo-B alloys were studied by X-ray diffraction, differential scanning calorimetry, transmission and high resolution electron microscopy and microhardness measurements. The nanocrystalline structure was produced by controlled crystallization of amorphous alloys. The annealed samples consist of the FCC nanocrystals with the amorphous regions between them. The grain size of the nanocrystals is about 20 nm and depends on the chemical composition of the alloy. The chemical composition of the amorphous phase between the nanocrystals changes at the annealing. A slight grain growth was observed when the annealing time increases. The diffusion of Mo and B from FCC to the amorphous phase occurs at the annealing. It results in the lattice parameter change. The microhardness of the alloys increases during the annealing. The microhardness values are the same in all alloys before the nanocrystalline structure decomposition. The microhardness is inconsistent with the Petch-Hall equation. The microhardness of the alloys is determined by the microhardness of the amorphous phase bands located between the nanocrystalline grains.

1. Introduction

The formation and development of new material are usually connected with the necessity of improved properties. New nanocrystalline materials appeared for this reason. Nanocrystalline alloys (with the grain size ≤ 50 nm) have aroused considerable interest because a large amount of the atoms in the nanocrystalline structure are located in the grain boundaries or interfaces. Nanocrystalline structure can be obtained by different methods: inert gas condensation [1], sputtering, mechanical alloying [2] or controlled crystallization of amorphous alloys [3, 4]. The last method was developed widely when it was found that the Fe-based nanocrystalline alloys posses the high soft magnetic properties [4]. More recently, the light Al- and Mg-based nanocrystalline alloys with the high strength were produced [5, 6].

Most mechanical properties are known to depend on the grain size. For example, yield strength and microhardness follow the Petch-Hall equation ($\sigma_\tau = \sigma_0 + K_y/\sqrt{d}$, where σ_τ is the yield strength, σ_0 is the lattice friction stress, K_y is a constant). Therefore the nanocrystalline materials with extremely small grain size attract particular interest from the standpoint of high strength properties. However, the Petch-Hall equation is not obeyed for the nanocrystalline alloys produced by the controlled crystallization [7, 8]. This may be due to a different deformation mechanism.

Ni-based nanocrystalline alloys with large content of Mo are very promising because of their high corrosion resistance and electrocatalytical properties [9]. High thermal stability is the other important property of nanocrystalline structure. The thermal stability of the nanocrystalline $(Ni_{65}Mo_{35})_{90}B_{10}$ alloy was found to be controlled by the thermal stability of remaining amorphous matrix [10]. The aim of this paper is to study the formation, structure and thermal stability and microhardness of the nanocrystalline structure in the of Ni-Mo-B system alloys and to investigate the structure/properties correlation.

2. Experimental methods

Amorphous $(Ni_{70}Mo_{30})_{90}B_{10}$ (1), $(Ni_{70}Mo_{30})_{95}B_5$ (2) and $(Ni_{65}Mo_{35})_{90}B_{10}$ (3), were prepared by melt quenching. Pure metals (>99.8%) have been used for the master alloy. The thickness of as-prepared ribbons was about 30 μm.

As-quenched amorphous alloys were studied by differential scanning calorimetry using a Perkin-Elmer system. The amorphous samples were annealed at 600 °C for 600 h in a vacuum furnace. The structure

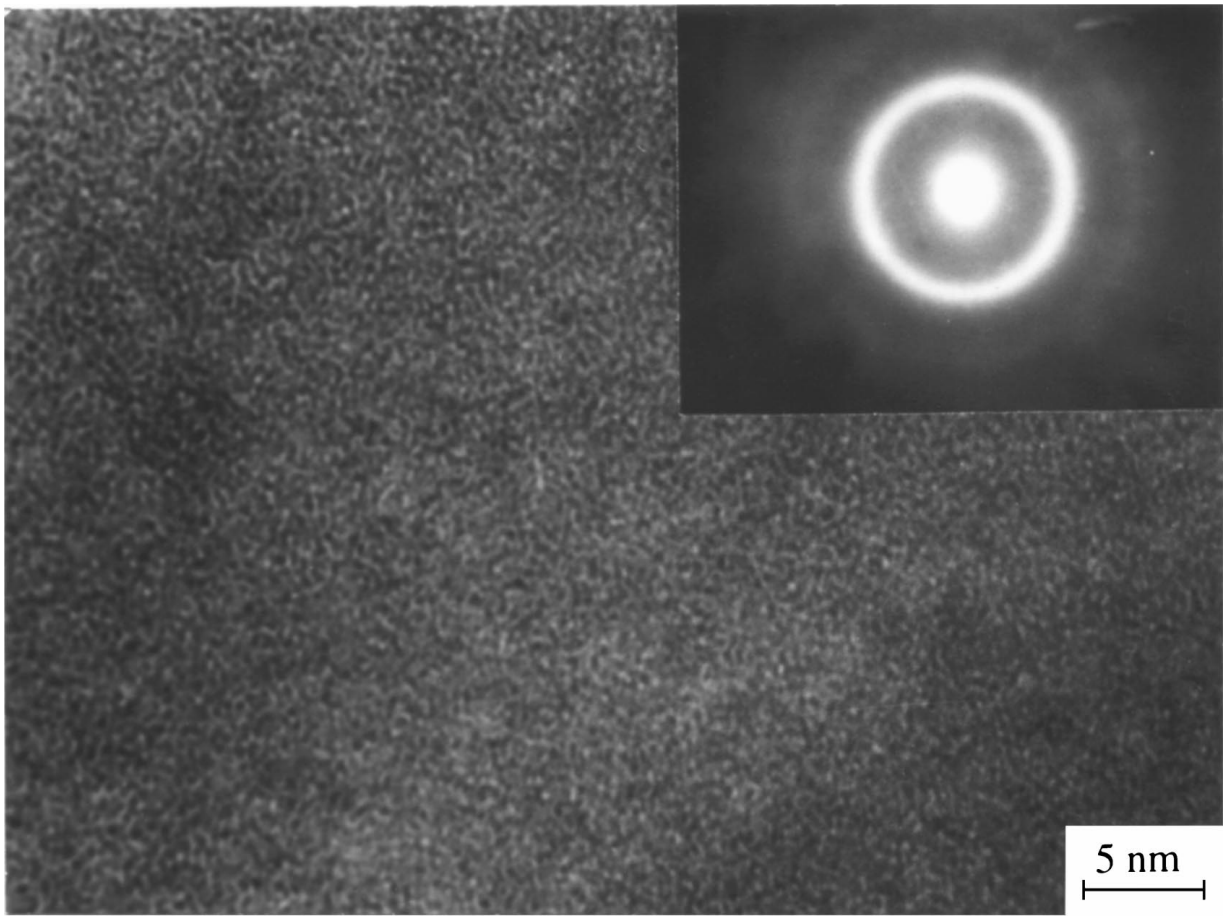

Figure 1 HREM image of as-prepared $(Ni_{65}Mo_{35})_{90}B_{10}$ alloy.

of as-quenched and annealed samples was studied by transmission and high resolution electron microscopy and X-ray diffraction. X-ray diffraction experiments were performed using SIEMENS D-500 diffractometer using CuK_α-radiation. The electron microscopy investigations were carried out on a JEOL-100 CX and JEOL 4000 EX ($C_s = 1.0$ mm, $U = 400$ kV) microscopes. Electron microscopy foils were prepared by ion milling from both sides of the ribbons.

The average grain size was estimated using Scherrer formula [11] by both from X-ray diffraction patterns and from dark field electron microscopy images. Special computer programs were used for the separation of the overlapped curves in the X-ray diffraction patterns and for the determination of the peak halfwidth. The diffraction experiments with Al standard were carried out for the determination of the lattice parameter change.

Vickers microhardness was measured using a microhardness tester (PMT-3) and a diamond pyramidal indentor with a 0.5 N load for the hold time of 20 s. All hardness measurements were taken at randomly selected places on the sample surface. An experimental error was about 3%.

3. Results

All as-quenched alloys {$(Ni_{70}Mo_{30})_{90}B_{10}$ (1), $(Ni_{70}Mo_{30})_{95}B_5$ (2) and $(Ni_{65}Mo_{35})_{90}B_{10}$ (3)} were amorphous. X-ray and electron diffraction patterns contain the diffuse halos only. A high resolution electron microscopy image of as-quenched $(Ni_{65}Mo_{35})_{90}B_{10}$ alloy is shown in Fig. 1. No signs of crystalline phases present the figure; only maze contrast typical for an amorphous structure is observed. An annealing at 600 °C leads to nanocrystalline structure formation in all alloys. The crystallization follows the primary crystallization mechanism. The annealed alloys contain Ni-based FCC nanocrystals with the chemical composition differing from those of as-quenched amorphous phase. The chemical composition of an amorphous matrix changes during the annealing as well.

Fig. 2 shows the DSC curves for the alloys 1 and 2. According to DSC measurements the crystallization temperatures are 829, 802 and 847 K for the alloy (1), (2), (3), respectively. Thus, the crystallization temperature rises with the increasing of the concentration of Mo or B.

The structure evolution at 600 °C is shown in Fig. 3. The structure of crystallized samples consists of FCC nanocrystals and amorphous phase. The part of nanocrystalline phase increases during the annealing. The lattice parameters of FCC nanocrystals depend on the annealing duration in all alloys. In $(Ni_{70}Mo_{30})_{90}B_{10}$ alloy the lattice parameter increases from 0.3592 to 0.3602 nm when the annealing time increases from 1 to 360 h. In $(Ni_{70}Mo_{30})_{95}B_5$ alloy the lattice parameter changes from 0.3593 to 0.3602 nm during the same heat treatment. In $(Ni_{65}Mo_{35})_{90}B_{10}$ alloy it decreases from

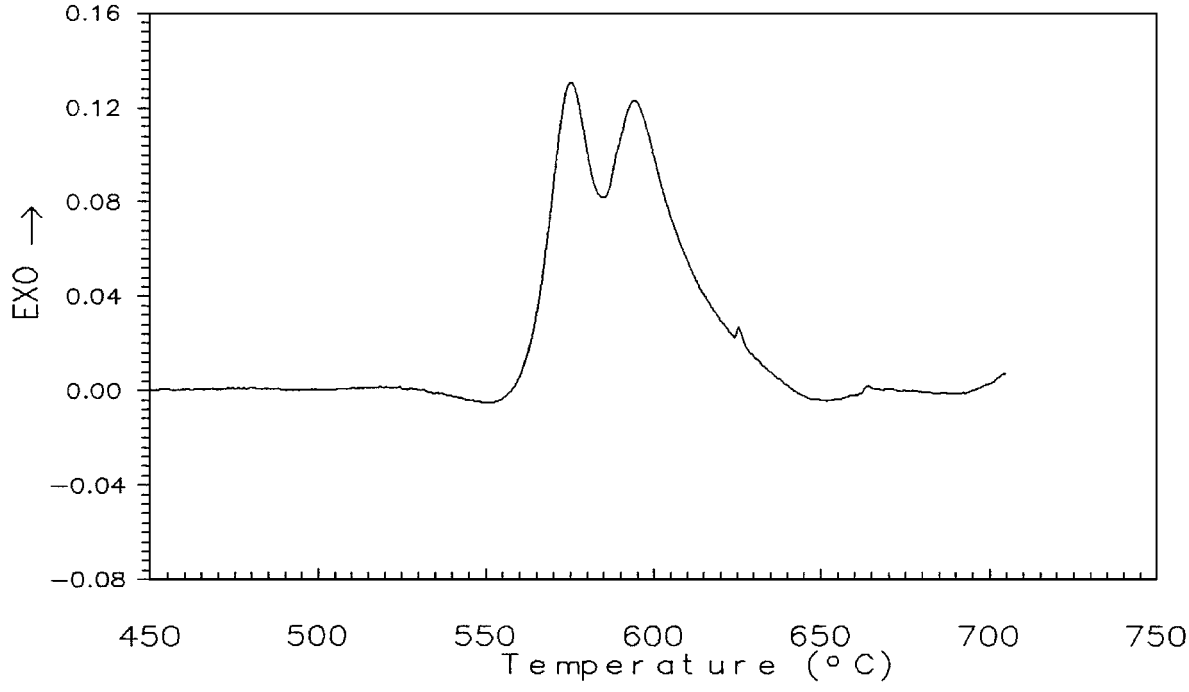

(a)

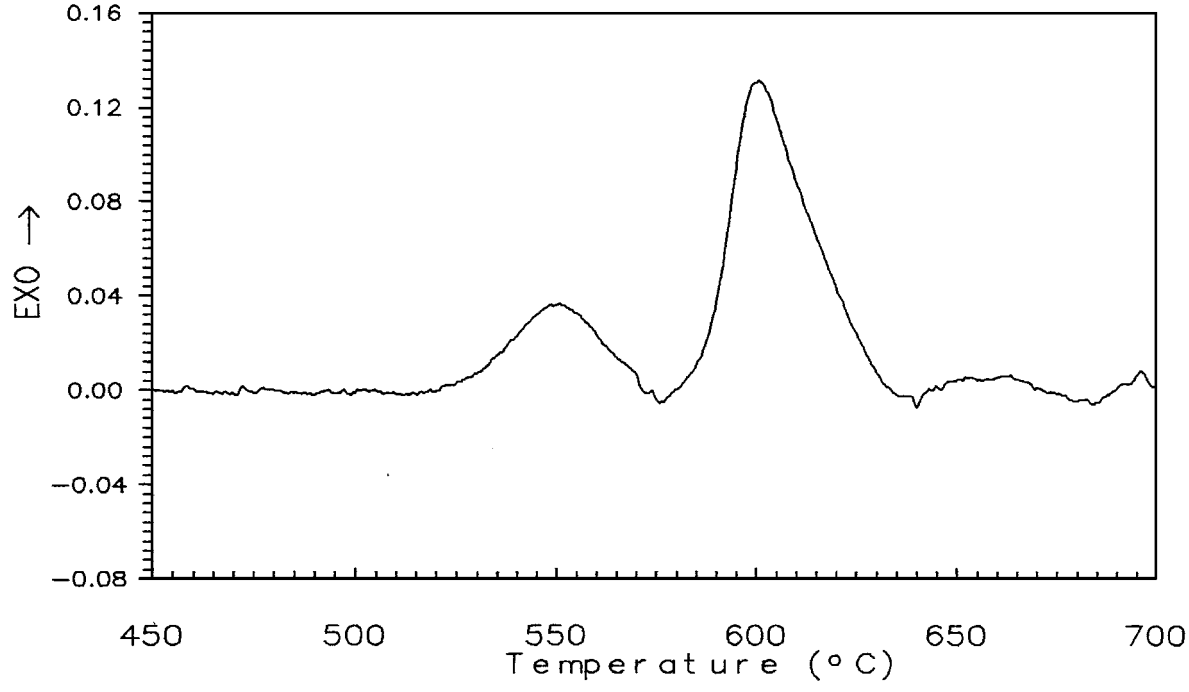

(b)

Figure 2 DSC data (20 K/min) for $(Ni_{70}Mo_{30})_{90}B_{10}$ (a) and $(Ni_{70}Mo_{30})_{95}B_5$ (b) alloys.

0.3600 to 0.3597 nm when the annealing time increases from 5 to 144 h.

When the annealing time increases above 240 h the nanocrystalline structure decomposes with Ni_3Mo, Mo_2B and Ni formation (the upper X-ray diffraction patterns in Fig. 3a, b). It is seen from these figures that the intensity of the nanocrystalline phase reflections decreases and the intensity of Ni_3Mo phase reflections increases when the nanocrystalline phase decomposes.

As it was mentioned above the crystallization leads to the formation of FCC nanocrystals representing a solid solution of Mo and B in Ni. The structure of annealed samples consists of two phases: FCC nanocrystals and amorphous matrix between them. The nanocrystals are separated from each other by the remaining amorphous phase. Fig. 4 shows the HREM image of this structure (the underfocusing was −49 nm and it corresponds to Scherzer defocusing). The average grain size increases slightly during the annealing at 600 °C and it practically does not change after the annealing more than 144 h. The dependencies of the grain sizes on the annealing time are shown in Fig. 5 for all alloys studied. The grain size shown in this figure is determined from TEM data.

The grain size does not exceed 28 nm, so we can conclude that all alloys have a nanocrystalline structure. This structure is shown in Fig. 6 for the

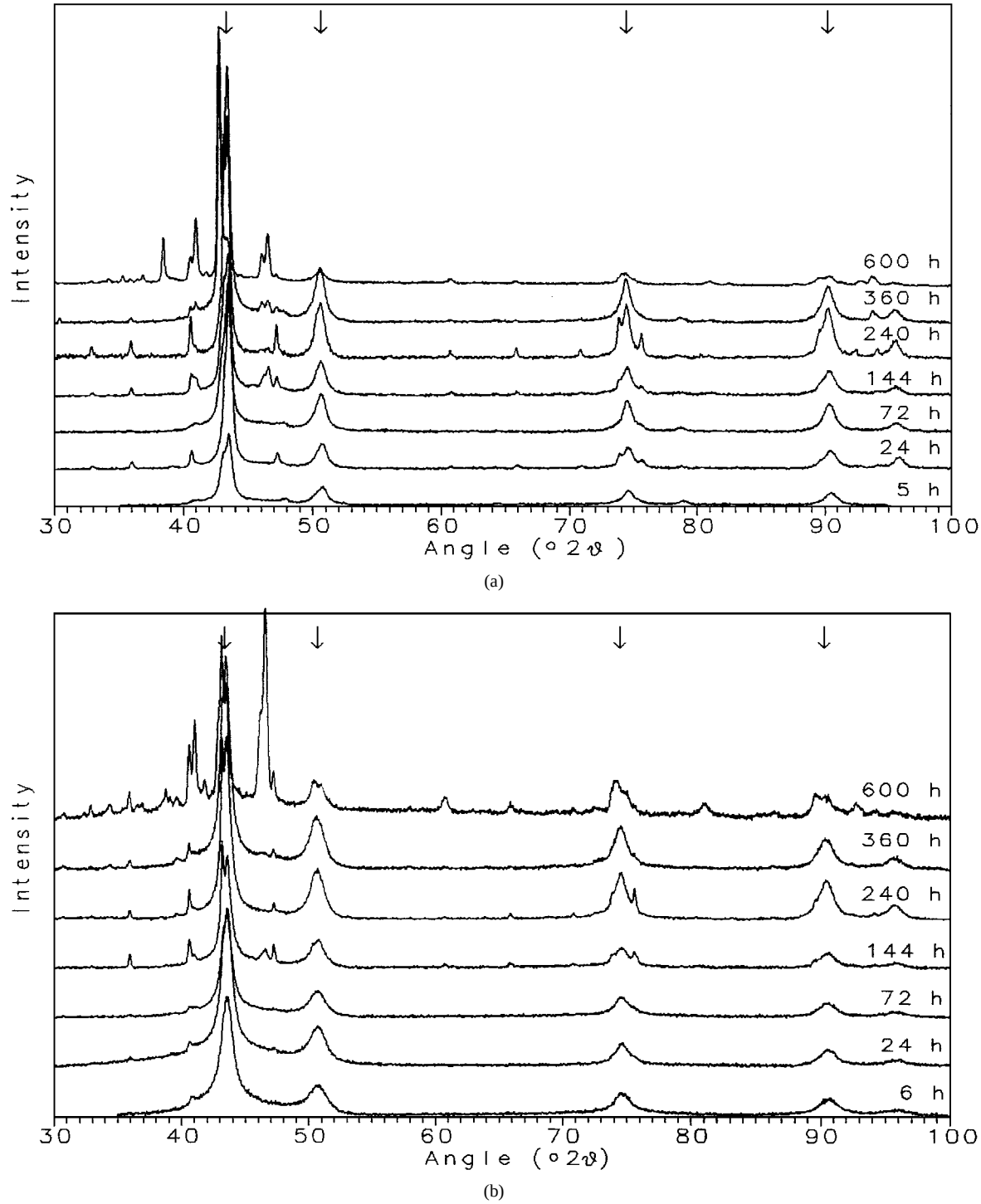

Figure 3 X-ray diffraction patterns of the alloys annealed at 600 °C: $(Ni_{70}Mo_{30})_{95}B_5$ (a), $(Ni_{70}Mo_{30})_{90}B_{10}$ (b). The arrows show the position of FCC phase reflections.

$(Ni_{70}Mo_{30})_{90}B_{10}$ alloy annealed for 24 h. According to the TEM data the grain size is about 15.5 nm in this sample. However, it is about 20 nm according to X-ray diffraction data. In order to clear the matter up we polished the sample surface to a depth of 8 μm. In this case the grain size determined from X-ray data is equal 16 nm. Due to the thinning process the TEM data is obtained from the central part of the samples. The lattice parameter is 0.3956 nm near the surface and it is 0.3954 nm at a depth of 8 μm.

The microhardness of the as-cast ribbons is highest in the ribbons with 10 at % B. The influence of an annealing treatment is shown in Fig. 7. The microhardness increases with the annealing time for all alloys studied and reaches the same value for all alloys after about 100 h. This dependence (Fig. 7) correlates with the dependence of grain size on the annealing time (Fig. 5). It should be noted that microhardness decreases sharply in all alloys when the nanocrystalline structure decomposes.

4. Discussion

As it was mentioned above, all as-prepared alloys were amorphous. According to DSC and structure investigation data the alloys crystallized by primary

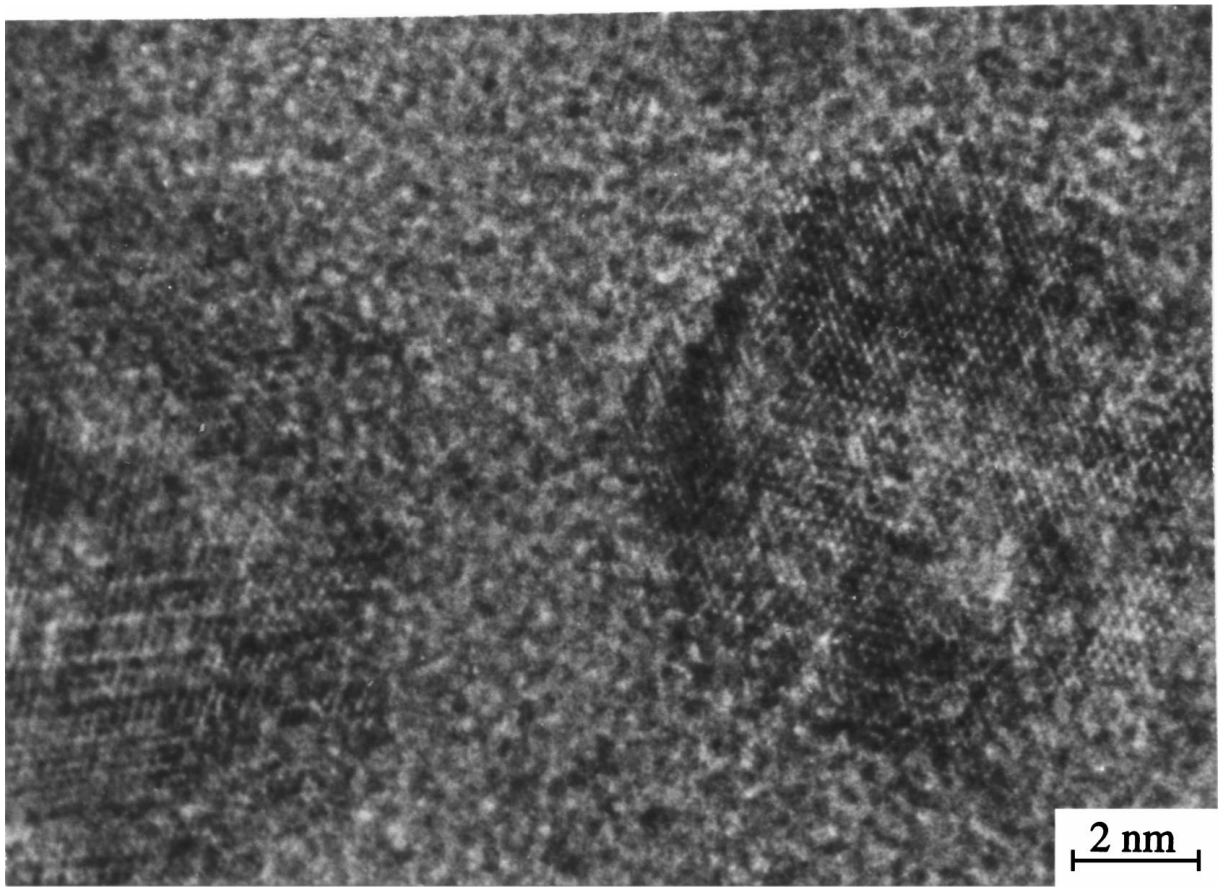

Figure 4 HREM image of $(Ni_{70}Mo_{30})_{90}B_{10}$ alloy annealed at 600 °C for 1 h.

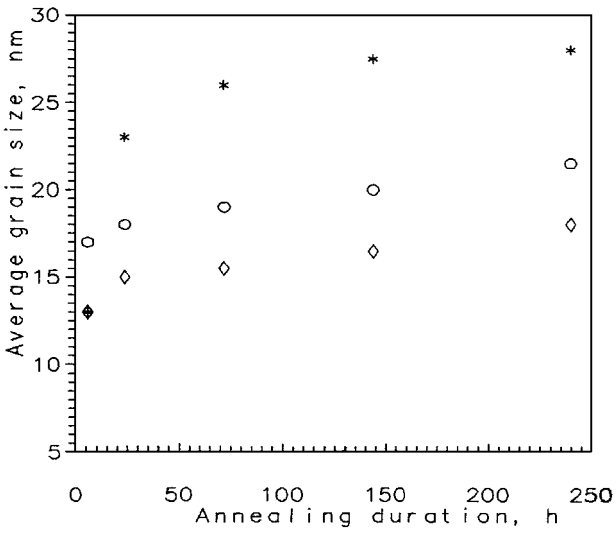

Figure 5 Change of the average grain size during the annealing of $(Ni_{70}Mo_{30})_{90}B_{10}$ (rhombs), $(Ni_{70}Mo_{30})_{95}B_5$ (circles) and $(Ni_{65}Mo_{35})_{90}B_{10}$ (stars) alloys.

crystallization mechanism at heating. The FCC crystals of Ni-based solid solution precipitate from an amorphous matrix on primary crystallization. Since chemical composition of the crystals formed during the primary crystallization differs from those of the matrix, chemical composition of remain amorphous phase changes during the crystallization. In our case the amorphous phase becomes enriched with Mo and B when the part of crystalline phase increases. On the other hand, the composition of precipitated crystals change during the annealing as well. The change of the nanocrystal composition leads to the lattice parameter change. As indicated above, the lattice parameter increases in $(Ni_{70}Mo_{30})_{90}B_{10}$, it does not practically change in $(Ni_{70}Mo_{30})_{95}B_5$ and slightly decreases in $(Ni_{65}Mo_{35})_{90}B_{10}$ alloy during the annealing. Mo is known to increase the lattice parameter of Ni, whereas incorporated B leads to a decrease. The observed change of lattice parameter can be explained as follows. The equilibrium concentration of the Mo in FCC-Ni is known to be 13.6 at % at 600 °C [12], the equilibrium concentration of the B in FCC is less than 1 at %. From the Thompson-Freundlich equation [13] it is known that very small crystals can solve a higher amount of solvent as compared to the stable phase diagram. Immediately after the formation the nanocrystals represent the supersaturated solid solution of Mo and B in FCC-Ni. It seems plausible that the chemical composition of the nanocrystals was different at the early stage of the annealing because of the difference in the chemical composition of the alloys. The different supersaturation of the nanocrystal lattice by Mo and B leads to the different values of the lattice parameters. The maximal value of the lattice parameter was observed in alloy with the greatest concentration of Mo ($(Ni_{65}Mo_{35})_{90}B_{10}$ alloy) and in the alloy with minimal boron concentration ($(Ni_{70}Mo_{30})_{95}B_5$ alloy). When the boron concentration increases (the $(Ni_{70}Mo_{30})_{90}B_{10}$ alloy in compare with $(Ni_{70}Mo_{30})_{95}B_5$ alloy) and the Mo concentration decreases (the $(Ni_{70}Mo_{30})_{90}B_{10}$ alloy in compare with

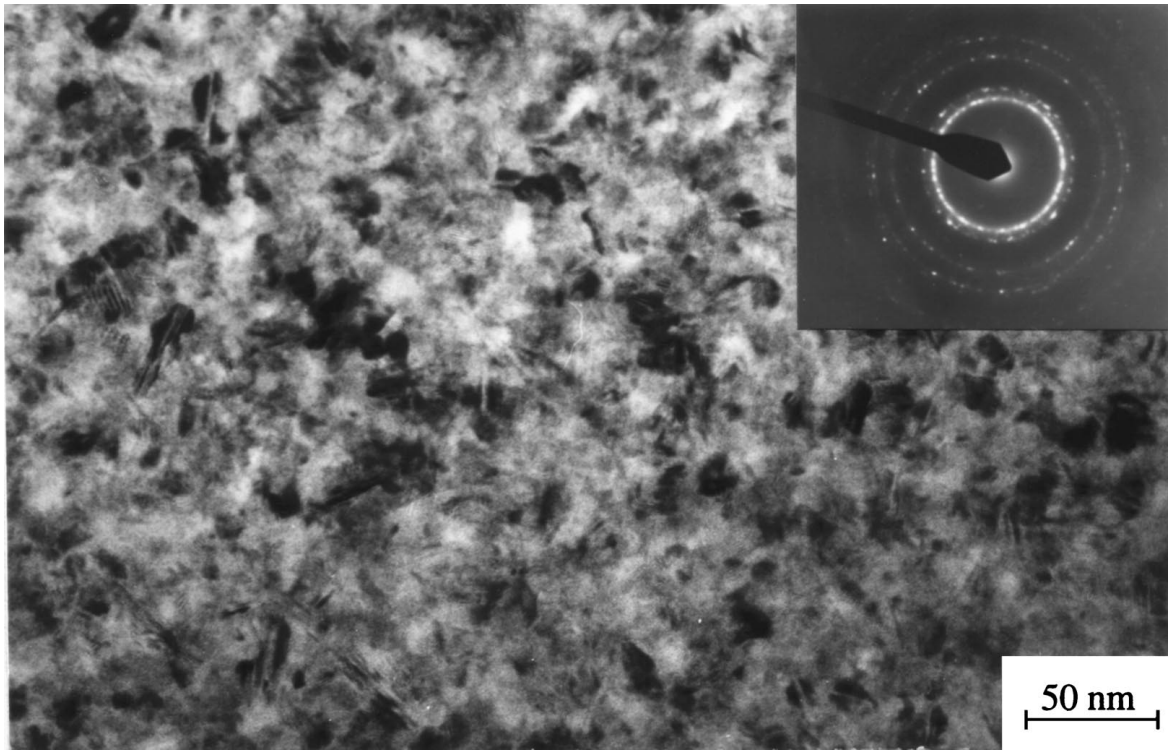

(a)

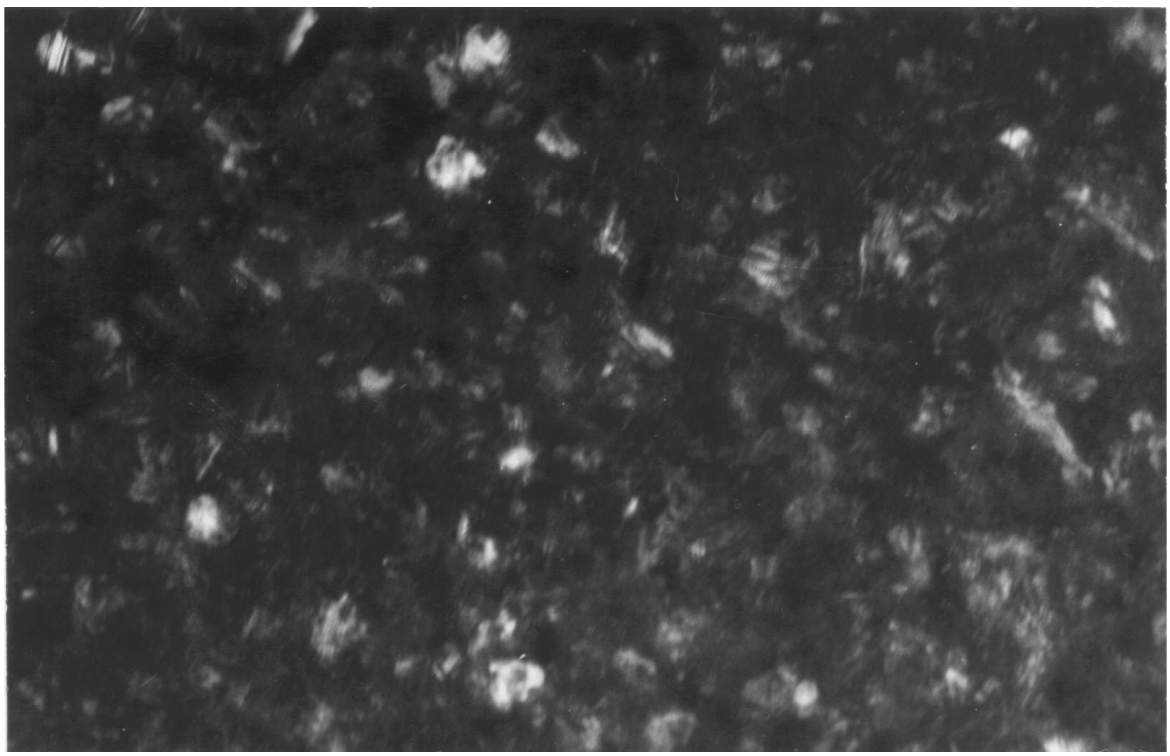

(b)

Figure 6 The structure of $(Ni_{70}Mo_{30})_{90}B_{10}$ alloy annealed for 24 h: bright field image (a) and dark field image (b).

$(Ni_{65}Mo_{35})_{90}B_{10}$ alloy), the nanocrystals form with the lesser lattice parameter. The simultaneous diffusion of Mo and B from the nanocrystals takes place during the annealing. The release of the largest amount of the Mo (together with the B) from the nanocrystals (in compare with the other alloys) leads to a slight decrease of the lattice parameter. Since the minimal amount of the Mo releases from the nanocrystals in $(Ni_{70}Mo_{30})_{90}B_{10}$ alloy, the lattice parameter should increase owing to the simultaneous diffusion of Mo and B, as it was observed. The nanocrystals in the $Ni_{70}Mo_{30})_{95}B_5$ alloy contain less amount of B then those in the other alloys and more amount of Mo than $(Ni_{70}Mo_{30})_{90}B_{10}$ alloy. Therefore the simultaneous diffusion of Mo and B does not lead to the appreciable change of the lattice parameter. It should be noted that all observed lattice parameters are more than the lattice parameter of the pure FCC-Ni (0.353 nm). It means that the nanocrystals contain the

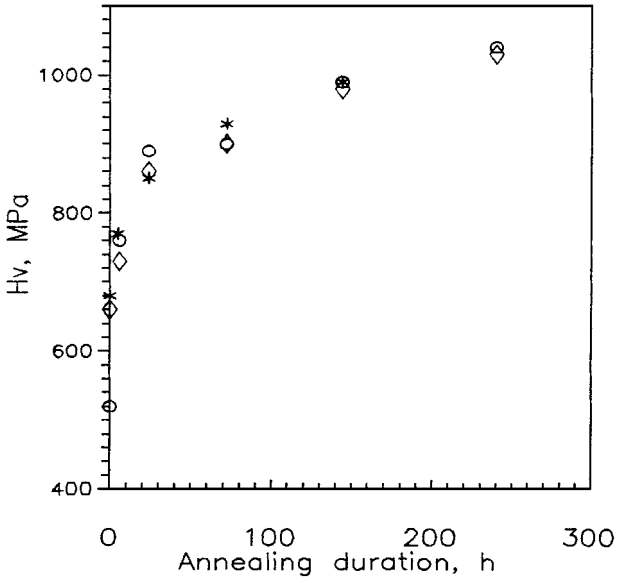

Figure 7 Microhardness dependence on annealing time for $(Ni_{70}Mo_{30})_{90}B_{10}$ (rhombs), $(Ni_{70}Mo_{30})_{95}B_5$ (circles) and $(Ni_{65}Mo_{35})_{90}B_{10}$ (stars) alloys.

large amount of Mo at the all stage of the nanocrystal existence. The molybdenum concentration in the nanocrystals estimated by the Vegard equation is about 20 at %. These estimations ignored the boron presence. It should be mentioned that the nanocrystal lattice parameter is practically the same in all alloys at the last stage of the nanocrystal existence; it allows to say about the same chemical composition of the nanocrystals.

It is significant that the grain size calculated from X-ray data (CuK_α-radiation, the penetration depth is about 4 μm for (111) reflection) was always larger than the grain size calculated from TEM data (information from the central part from the samples). The X-ray diffraction and TEM data coincide when the sample surface was polished (to a depth of 8 μm). The lattice parameter changes in this case as well. This difference in the grain size (and lattice parameter) can be due to the different chemical composition in the near surface layer and in the bulk. The lattice parameter decreasing with the depth increase was suggested to be attributed to the depletion in B of the near surface layer. As illustrated in Fig. 5, the grain size of the nanocrystalline structure increases when the boron concentration decreases from 10 to 5 at %. Therefore one would expect the increasing of the grain size (and the lattice parameter) with the depletion of the near surface layer in boron.

The nanocrystalline structure has a high thermal stability in the studied alloys. The average grain size is about 15–25 nm depending on the heat treatment. The annealing temperature T_a is about $0.6T_m$ (T_m is melting temperature), this temperature is high enough for the recrystallization process in usual alloys with the fine grains [14]. However, marked grain growth was not observed. Let us consider a possible reason. The grain size increases during the annealing. This increase is pronounced at the early stages of annealing, then the grain size is practically constant. The amorphous matrix becomes enriched with Mo and B with annealing time increase. The amorphous matrix locates between the nanocrystal grains so that it seals the grains off from each other and prevents the nanocrystal growth at the cost of each other. In such a manner the amorphous matrix determines the thermal stability of the nanocrystalline structure. As the data of DSC suggest (Fig. 2), the crystallization temperature of the amorphous alloys increases with the increase of Mo and B concentrations. So, the chemical composition of the amorphous matrix changes during the annealing resulting in a increasing of its crystallization temperature, i.e., thermal stability. In Fe-B metallic glasses it is known that Mo additions increase the crystallization temperature significantly [15].

The study of the nanocrystalline structure evolution to the point of the decomposition has a significant place in the analysis of the structure stability. It is not clear yet what phases form from the nanocrystals, what phases form from the amorphous matrix. In all alloys the nanocrystalline structure decomposition leads to the formation of Ni_3Mo, Mo_2B and a small amount of Ni. According to the X-ray diffraction during decomposition of the nanocrystalline phase the amount of FCC phase has been observed to decrease at the same time when the Ni_3Mo phase is formed. Therefore, the Ni_3Mo phase forms probably from the nanocrystalline supersaturated solid solution. The Ni is known to exhibit a FCC lattice (Fm3m space group) [16] which can be described as a three-layer packing: . . .ABCABC. . . with dense-packed layers perpendicular to [111] direction. The Ni_3Mo phase has the distorted two-layer hexagonal packing (Pmmn space group). In this lattice the dense-packed layers form a . . .ABABAB. . . sequence perpendicular to the [010] direction and consist of Ni and Mo atoms, they are distorted through the size effect. The transition from FCC supersaturated solid solution to the Ni_3Mo phase structure is possible by the shift of the hexagonal layers of the FCC solid solution and the change of the three-layer hexagonal ABCABC. . . packing to the two-layer ABAB. . . packing. The atom displacement is 0.0147 nm at the shift, this distance is significantly shorter than the lattice parameter. The transition from FCC supersaturated solid solution to the Ni_3Mo phase structure can proceed for example by dislocation mechanism as in the well known Co transformation [17]. It should be noted that the Ni-based nanocrystalline phase has a numerous twins and stacking faults [18] and the stacking faults in FCC structure are known to be the part of the HCP structure. Moreover, such transition requires an insignificant diffusion redistribution of the alloy components because the Mo concentration in the solid solution is close to the Mo concentration in the Ni_3Mo phase. For a final conclusion whether the decomposition of the nanocrystalline structure and formation of the Ni_3Mo phase proceeds by a dislocation mechanism or by nucleation and growth further investigations are necessary.

The change of microhardness during the annealing is shown in Fig. 7. The microhardness of all alloys increases with the increasing of the annealing duration (and with the increasing of the grain size). Since the yield strength $\sigma_\tau \approx H_v/3$, it means that the observed

dependence of the yield strength on the grain size is inverse to the Petch-Hall equation ($\sigma_\tau = \sigma_0 + K_y/\sqrt{d}$, where σ_τ is the yield strength, σ_0 is the friction stress required to move individual dislocation independing on the grain size, K_y is a positive constant of yielding associated with the stress required to extend dislocation activity into adjacent unyielded grains [19]. Therefore, the Petch-Hall equation may be replaced by $H_v = H_o + K_h/\sqrt{d}$, where H_v and K_h are appropriate constants associated with the hardness measurements. The experimental dependence obtained is not explainable on a basis of dislocation interactions (Petch-Hall equation). The inconsistentence with the Petch-Hall equation was observed in [7] for the nanocrystalline alloys produced by controlled crystallization of amorphous Zr-based alloys. Authors of papers [6, 7] assumed that the microhardness of the nanocrystalline alloys is influenced by the presence of an amorphous matrix. In our case it is also reasonable to suggest that the alloy strength can be attributed to the strength of amorphous matrix. We assume that the strengthening of the amorphous matrix results from the alloy component redistribution when the crystals form and grow. The amorphous matrix enriches in Mo and B during the annealing which leads to a strenthening. An alloy (crystalline as well as amorphous) with the higher concentration of B and Mo exhibit a higher hardness (see for example the initial points in Fig. 7). The composition of the remaining amorphous matrixes should be similar in all alloys studied, but the volume fraction depends on the concentration of B and Mo in the as-cast alloy. This should lead to a higher hardness of the alloys with more B or Mo. On the other hand, it should be noted that the microhardness is practically the same (with regard to the experimental errors) in all alloys at the stage of the "stable" nanocrystalline structure although grain sizes are different. The largest grain size which was observed in the alloy with highest content of B and Mo should result in the lowest hardness. These two opposite effects are assumed to compensate each other.

5. Conclusions

1. Crystallization of amorphous $(Ni_{70}Mo_{30})_{90}B_{10}$, $(Ni_{70}Mo_{30})_{95}B_5$ and $(Ni_{65}Mo_{35})_{90}B_{10}$ alloys at 600 °C leads to the formation of nanocrystalline structure; the nanocrystal size is 15–25 nm and increases slightly with the annealing time.

2. The lattice parameters of nanocrystals depend on the alloy composition and the annealing duration: Whereas in $(Ni_{70}Mo_{30})_{90}B_{10}$ and in $(Ni_{70}Mo_{30})_{95}B_5$ an increase was observed, a slight decrease in $(Ni_{65}Mo_{35})_{90}B_{10}$ was found. These changes are attributed to the different initial composition of the nanocrystals and to the simultaneous diffusion of Mo and B from the nanocrystals to the amorphous matrix.

2. The stability of the nanocrystalline structure results from the thermal stability of the amorphous matrix which insulate the grains from each other; the crystallization temperature of amorphous matrix increases during the annealing owing to the enriching with B and Mo.

3. The microhardness has been observed to increase when the nanocrystalline structure is formed and increases further with the growth of the nanocrystals. This behavior is inverse to Petch-Hall law and it may be explained by the increase of the B and Mo content in the amorphous matrix.

4. The nanocrystalline structure decompose during further annealing into the equilibrium phases: Ni_3Mo, Mo_2B and Ni. The Ni_3Mo phase may be formed from the nanocrystalline solid solution.

Acknowledgement

This work was performed as a part of the projects 96-02-19582 (RBRF). Financial support of RBRF is gratefully acknowledged. The authors are grateful to Dr. A. Gurov for DSC measurements.

References

1. H. GLEITER, *Prog. Mater. Sci.* **33** (1989) 223.
2. C. C. KOCH, *Nanostr. Mater.* **2** (1993) 109.
3. Y. YOSHIZAWA, K. YAMAUCHI and S. OGUMA, European Patent EP 0,271,657 A2 (1987).
4. U. KÖSTER, U. SCHUHEMANN, M. BLANK-BEWERSDORF, S. BRAUER, M. SUTTON and G. P. STEPHENSON, *Mater. Sci. Eng.* **A133** (1991) 611.
5. P. ALLIA, C. BEATRICE, F. VINAI, M. KNOBEL and T. R. SATO, *Appl. Phys. Lett.* **59** (1991) 2454.
6. Z. C. ZHONG, X. Y. JIANG and A. L. GREER, *Mater. Sci. Eng.* **A226–228** (1997) 531.
7. H. ALVES, M. FERREIRA, U. KÖSTER and B. MÜLLER, *Mater. Sci. Forum* **225–227** (1996) 769.
8. X. D. LIU, J. T. WANG, Z. Q. HU and B. Z. DING, *Mater. Sci. Eng.* **169A** (1993) L17.
9. H. ALVES, M. FEREIRA and U. KÖSTER, *Mater. Sci. Forum* **179–181** (1995) 449.
10. A. S. ARONIN, G. E. ABROSIMOVA, I. I. ZVER'KOVA, YU. V. KIR'JANOV, V. V. MOLOKANOV and M. I. PETRZHIK, *Mater. Sci. Eng.* **A226–228** (1997) 536.
11. A. GUINIER, "Theorie et technique de la radiocristallographie" (Dumond, Paris, 1956).
12. P. ELLIOTT, "Constitution of Binary Alloys, First Supplement" (Metallurgia, Moscow, 1970).
13. R. A. SWALIN, "Thermodynamics of Solids" (John Wiley & Sons, New York, 1972).
14. S. S. GORELIK, "Recristallizacija metallov i splavov" (Mettallugia, Moscow, 1978).
15. U. HEROLD and U. KÖSTER, in Proceedings of RQ3 (The Metal Society, London, 1978) p. 281.
16. Pearson's Handbook of Crystallographic Data for Intermetallic Phases, edited by P. Villars and L. D. Calvert (American Society for Metals, Metals Park, OH 44073, 1986) Vol. 3, p. 3528.
17. A. SEEGER, *Z. Metallkunde* **44** (1953) 247.
18. G. E. ABROSIMOVA, A. S. ARONIN, I. I. ZVER'KOVA, YU. V. KIR'JANOV, V. V. MOLOKANOV and M. I. PETRZHIK, *Poverhnost* **7** (1996) 84.
19. J. HIRTH and J. LOTHE, "Dislocation Theory" (Atomizdat, Moscow 1972).

Received 14 August 1997
and accepted 26 October 1998